Structure factor of hard spheres near a wall

B. Götzelmann, A. Haase, and S. Dietrich
Fachbereich Physik, Bergische Universität Wuppertal, D-42097 Wuppertal, Germany
(Received 9 November 1995)

Within a certain version of weighted density functional theory we have determined the direct correlation function of a hard sphere fluid close to a hard wall and, based on the Ornstein-Zernicke equation, its inverse yielding the structure factor. We compare these results as well as the corresponding density profiles with those obtained from the inhomogeneous Percus-Yevick theory and from published simulation data. We find a good quantitative agreement at low and medium densities which also persists, apart from some amplitudes, at higher densities. In addition we have computed the excess coverage and the surface tension.

PACS number(s): 61.20.Ne, 68.45.−v, 68.10.Cr, 05.70.−a

I. INTRODUCTION

The interest in interfaces is based on the fact that they induce a spatial variation, normal to their positions, of most correlation functions characterizing the structural properties of condensed matter. Due to significant theoretical and experimental challenges, up to now the overwhelming majority of the research efforts in this area has been devoted to determining the spatial variation of *one-point* correlation functions, such as number densities profiles, magnetization profiles, or orientational profiles, and their corresponding integral excess quantities. This situation is caused mainly by the fact that practically all surface specific experimental techniques, if they provide depth resolution in the first place, render first one-point correlation functions but rarely higher order correlation functions.

In the ordered bulk, however, one-point correlation functions are either constant, as in fluids, or display a periodic crystallographic arrangement of the constituents. A significantly deeper insight into the structural properties is provided by the two-point correlation function, i.e., the structure factor, which in the bulk is probed directly by x-ray and neutron scattering experiments.

Obviously one is interested in extending the same level of describing condensed matter to the interfacial region. This goal can be achieved by using recently available powerful x-ray and neutron sources which allow one to perform scattering experiments under grazing incidence, and thus to extract relevant structural information about interfaces. By varying the incident or exit angles of the beam, the depth profile of the lateral structures can be studied. These ideas have been implemented successfully, e.g., for determining the critical two-point correlation function of the order parameter near the surface of a solid undergoing a continuous phase transition in the bulk [1–3]. Since any correlation function between points $\mathbf{R}_1=(\mathbf{r}_1,z_1)$ and $\mathbf{R}_2=(\mathbf{r}_2,z_2)$, where z_1 and z_2 denote their relative normal distances from the mean interface position, depends on $\mathbf{r}_{12}=\mathbf{r}_1-\mathbf{r}_2$, z_1, and z_2, whereas there is only one lateral momentum transfer $\mathbf{p}$ available, it is clear that one needs theoretical guidance in order to determine the full structure factor from varying $\mathbf{p}$ and the scattering geometry. In contrast to the bulk, where scattering experiments yield the Fourier transform of the two-point correlation function directly, at the surface one measures its Fourier transform with respect to $\mathbf{r}_{12}$, but the Laplace transform with respect to z_1 and z_2 which cannot be inverted directly [4].

The present contribution intends to provide a first step in this theoretical guidance for investigating the two-point correlation function of fluids close to their confining walls. This first step consists of the study of hard spheres close to a hard wall. The choice of this system has four virtues.

(i) The solution of this problem is a prerequisite [5–7] for comprehensive studies of fluids with attractive and soft repulsive interactions which may exhibit phase transitions like wetting phenomena [8] characterized by long-ranged lateral correlations.

(ii) It is well suited for comparing analytical approaches with simulation data. In fluids governed by long-ranged forces, such a comparison is less reliable because it is more difficult to incorporate such forces into simulations. In density functional theory the perturbative incorporation of attractive interactions tends to be easier once the hard sphere reference system is well understood.

(iii) In dense fluids, correlations at short distances are dominated by the repulsive forces between the particles, so that the results for the reference system of hard spheres renders already important insights into the structures of actual fluids.

(iv) The relevant theoretical results for this model system do not depend on the absolute value of the diameter of the spheres. Therefore these results can also be applied to colloidal particles which under favorable circumstances closely resemble an effective model of hard spheres [9]. Their structure factor is even accessible by light scattering. On the scale of the diameter of colloidal particles, the actual atomic corrugation of the container walls is a minor perturbation of a flat wall, so that this latter aspect of the theoretical model represents a reasonable approximation of these systems.

So far the two-point correlation function (or the so-called total correlation function) of hard spheres near a hard wall has been studied either by simulations [10–12] or by integral equation methods [13–16]. Since the latter approaches are known to fail in describing particular interesting interfacial phase transitions such as wetting phenomena, we set out to determine the two-point correlation function based on a certain version of weighted density functional theory which is known to capture wetting transitions. Thus in a later stage

this approach enables one to build on the present results in order to describe two-point correlation functions near such phase transitions. Since in the hard sphere system the correlation functions vary rapidly on the scale of the diameter of the spheres, one must resort to numerically more demanding weighted density approximations (WDA's) as opposed to the often used local density approximation (LDA). So far for WDA density functionals the total correlation function has been determined only in the bulk [17,18].

In the following we first discuss the basic equations determining the total correlation function (Sec. II). In Sec. III we describe the WDA used in our approach. Our results are presented in Sec. IV, and summarized in Sec. V.

II. DENSITY FUNCTIONAL THEORY

A. Basic equations for correlation functions

The equilibrium density profile $\rho(\mathbf{R};T,\mu,V)$ of an inhomogeneous liquid exposed to an external potential $V(\mathbf{R})$ minimizes the grand potential functional [7,19]

$$\Omega([\tilde{\rho}(\mathbf{R})];T,\mu,V)=F([\tilde{\rho}(\mathbf{R})];T,V) - \int_V d^3R[\mu-V(\mathbf{R})]\tilde{\rho}(\mathbf{R}) \quad (2.1)$$

as a function of the chemical potential μ, the temperature $T=1/(k_B\beta)$, and the size V of the system. The Helmholtz free-energy functional $F[\tilde{\rho}]$ depends parametrically on the interaction potential between the particles but not on $V(\mathbf{R})$. After subtracting the ideal gas contribution $F_{\rm id}[\tilde{\rho}]=(1/\beta)\int_V d^3R\tilde{\rho}(\mathbf{R})[\ln(\Lambda^3\rho(\mathbf{R}))-1]$, it defines the hierarchy of the so-called direct correlation functions:

$$c^{(1)}(\mathbf{R};[\tilde{\rho}]):=-\beta\frac{\delta(F[\tilde{\rho}]-F_{\rm id}[\tilde{\rho}])}{\delta\tilde{\rho}(\mathbf{R})} \quad (2.2)$$

and

$$c^{(2)}(\mathbf{R}_1,\mathbf{R}_2;[\tilde{\rho}]):=-\beta\frac{\delta^2(F[\tilde{\rho}]-F_{\rm id}[\tilde{\rho}])}{\delta\tilde{\rho}(\mathbf{R}_1)\delta\tilde{\rho}(\mathbf{R}_2)}. \quad (2.3)$$

Thus the minimum $\tilde{\rho}=\rho$ of the grand potential $\Omega[\tilde{\rho}]$ is determined by

$$c^{(1)}(\mathbf{R};[\rho])-\ln(\Lambda^3\rho(\mathbf{R}))+\beta u(\mathbf{R})=0. \quad (2.4)$$

Λ is the thermal de Broglie wavelength, and $u(\mathbf{R})=\mu-V(\mathbf{R})$. In Eq. (2.4), $u(\mathbf{R})$ can be considered as a functional of $\rho(\mathbf{R})$, so that further differentiation leads to

$$c^{(2)}(\mathbf{R}_1,\mathbf{R}_2)=\frac{\delta(\mathbf{R}_1-\mathbf{R}_2)}{\rho(\mathbf{R}_1)}-\beta\frac{\delta u(\mathbf{R}_1)}{\delta\rho(\mathbf{R}_2)}. \quad (2.5)$$

On the other hand, functional derivatives of the equilibrium grand partition function $\Omega[\rho]$ yield the hierarchy of the n-body distribution functions $\rho^{(n)}(\mathbf{R}_1,\ldots,\mathbf{R}_n)$:

$$\frac{\delta\Omega}{\delta u(\mathbf{R}_1)}=-\rho(\mathbf{R}_1)=-\langle\hat{\rho}(\mathbf{R}_1)\rangle \quad (2.6)$$

and

$$-\frac{1}{\beta}\frac{\delta^2\Omega}{\delta u(\mathbf{R}_1)\delta u(\mathbf{R}_2)}=\frac{1}{\beta}\frac{\delta\rho(\mathbf{R}_1)}{\delta u(\mathbf{R}_2)}=G(\mathbf{R}_1,\mathbf{R}_2) =:\rho^{(2)}(\mathbf{R}_1,\mathbf{R}_2)-\rho(\mathbf{R}_1)\rho(\mathbf{R}_2) +\rho(\mathbf{R}_1)\delta(\mathbf{R}_1-\mathbf{R}_2) =:h(\mathbf{R}_1,\mathbf{R}_2)\rho(\mathbf{R}_1)\rho(\mathbf{R}_2) +\rho(\mathbf{R}_1)\delta(\mathbf{R}_1-\mathbf{R}_2), \quad (2.7)$$

where

$$G(\mathbf{R}_1,\mathbf{R}_2)=\langle\hat{\rho}(\mathbf{R}_1)\hat{\rho}(\mathbf{R}_2)\rangle-\langle\hat{\rho}(\mathbf{R}_1)\rangle\langle\hat{\rho}(\mathbf{R}_2)\rangle \quad (2.8)$$

denotes the experimentally accessible two-point correlation function in terms of the thermal average $\langle\ \rangle$ of the fluctuating number density $\hat{\rho}(\mathbf{R})=\Sigma_i\delta(\mathbf{R}-\mathbf{R}_i)$ of the particles. The total correlation function $h(\mathbf{R}_1,\mathbf{R}_2)=[G(\mathbf{R}_1,\mathbf{R}_2)-\rho(\mathbf{R}_1)\delta(\mathbf{R}_1,\mathbf{R}_2)]/(\rho(\mathbf{R}_1)\rho(\mathbf{R}_2))$, and the direct correlation function $c^{(2)}(\mathbf{R}_1,\mathbf{R}_2)$ can be related by substituting Eqs. (2.5) and (2.7) into

$$\delta(\mathbf{R}_1-\mathbf{R}_2)=\int d^3R_3\frac{\delta u(\mathbf{R}_1)}{\delta\rho(\mathbf{R}_3)}\frac{\delta\rho(\mathbf{R}_3)}{\delta u(\mathbf{R}_2)}, \quad (2.9)$$

resulting into the Ornstein-Zernicke (OZ) equation

$$h(\mathbf{R}_1,\mathbf{R}_2)=c^{(2)}(\mathbf{R}_1,\mathbf{R}_2)+\int d^3R_3 \times c^{(2)}(\mathbf{R}_1,\mathbf{R}_3)\rho(\mathbf{R}_3)h(\mathbf{R}_3,\mathbf{R}_2). \quad (2.10)$$

Based on this equation there are two approaches to computing the total correlation function of the system. In the first one a closure relation is employed which renders a second relationship between the direct and total correlation functions. In the case of a hard sphere fluid the Percus-Yevick approximation (PY) has been found to be reliable at least for homogeneous systems [20]:

$$y(\mathbf{R}_1,\mathbf{R}_2)=h(\mathbf{R}_1,\mathbf{R}_2)+1-c^{(2)}(\mathbf{R}_1,\mathbf{R}_2) =g(\mathbf{R}_1,\mathbf{R}_2)-c^{(2)}(\mathbf{R}_1,\mathbf{R}_2), \quad (2.11)$$

where $y(\mathbf{R}_1,\mathbf{R}_2)=\exp(\beta\Phi(|\mathbf{R}_1-\mathbf{R}_2|))[h(\mathbf{R}_1,\mathbf{R}_2)+1]$. The radial distribution function is defined as $g=h+1$. For hard spheres the particle-particle interaction potential $\Phi(r)$ is infinite if the spheres overlap, and zero otherwise. Exploiting an additional exact relation like the Lovett-Mou-Buff-Wertheim equation [21] or the first Born-Green-Yvon (BGY) equation [20]

$$\frac{1}{\beta}\frac{1}{\rho(\mathbf{R}_1)}\nabla_{\mathbf{R}_1}\rho(\mathbf{R}_1)=-\nabla_{\mathbf{R}_1}V(\mathbf{R}_1)-\int d^3R_2\rho(\mathbf{R}_2) \times[h(\mathbf{R}_1,\mathbf{R}_2)+1]\nabla_{\mathbf{R}_1}\Phi(\mathbf{R}_{12}), \quad (2.12)$$

one can determine $h(\mathbf{R}_1,\mathbf{R}_2)$ by simultaneously iterating one of these sets of three coupled integral equations for $h(\mathbf{R}_1,\mathbf{R}_2)$, $c^{(2)}(\mathbf{R}_1,\mathbf{R}_2)$, and $\rho(\mathbf{R})$ [13–16,22]. Within this approach for a *homogeneous* fluid explicit analytic expres-

sions [23] for the PY approximations of the free energy, the pressure, the direct correlation function

$$c_{\mathrm{PY}}(R)=\frac{1}{(1-\eta)^4}\left[-(1+2\eta)^2+\tfrac{3}{2}\eta(2+\eta)^2\frac{R}{\sigma}-\tfrac{1}{2}\eta(1+2\eta)^2\frac{R^3}{\sigma^3}\right]\Theta(|\sigma-R|), \tag{2.13}$$

and, in a restricted range of R, of the total correlation function $h_{\mathrm{PY}}(R)$ [24] are known; σ is the diameter of the spheres and $\eta=(\pi/6)\rho\sigma^3$ the packing fraction.

Within the second approach an ansatz for $F[\tilde{\rho}]$ enables one to use Eq. (2.3) in order to obtain $c^{(2)}(\mathbf{R}_1,\mathbf{R}_2)$ directly, from which $h(\mathbf{R}_1,\mathbf{R}_2)$ follows via the OZ equation (2.10). Since $F_{\mathrm{ex}}[\tilde{\rho}]=F[\tilde{\rho}]-F_{\mathrm{id}}[\tilde{\rho}]$ is not known exactly, this ansatz requires one to find an appropriate approximation thereof. Within the framework of the often used local density approximation (LDA), $c^{(2)}(\mathbf{R}_1,\mathbf{R}_2)$ reduces to Dirac's δ function, and all excluded volume effects are missed. If one incorporates attractive interactions between the particles within the LDA, only general results for the long-ranged part of the correlations can be obtained [25,26]. But for a hard sphere fluid there are only short-ranged correlations, and therefore a more sophisticated approximation for $F_{\mathrm{ex}}[\tilde{\rho}]$ is to be chosen.

B. Linear weighted density approximation

There is a large variety of different WDA's known in the literature [7]. Some of them are designed to describe the freezing transition in the bulk, which at present is not our focus. There are many other approximations which deal specifically with the problem of describing the fluid structure near a hard wall. With variable success the density profile close to the wall as obtained by simulations is reproduced, and as a rule increasing accuracy demands greater numerical efforts. For our goal it is important to choose an approach which reproduces the density profile satisfactorily, but is numerically not too demanding, as we want to determine higher order correlation functions. In view of these aims we have based our calculations on the linear weighted density approximation (LWDA) introduced by Ohnesorge [27]. Initially this was introduced with the intention of describing freezing of hard spheres, which occurs at $\rho_b\sigma^3\simeq 0.94$ [28], but within this approach the actual fcc crystal structure turned out to be unstable with respect to the simple cubic (sc) structure. However, in spite of this failure close to the freezing transition the density profile in the vicinity of a hard wall is reproduced satisfactorily (see, cf., Sec. III). Moreover, this approach is very appealing because its numerical implementation is relatively easy.

As a generalization of the original spirit of the WDA, in the LWDA a *set* of weighted densities is introduced,

$$\bar{\rho}_\nu(\mathbf{R}_1)=\int \bar{\omega}_\nu(|\mathbf{R}_1-\mathbf{R}_2|)\rho(\mathbf{R}_2)d^3R_2, \tag{2.14}$$

with normalized weights $\bar{\omega}_\nu(r)$, $\nu=0,\ldots,3$. Their construction is constrained by the requirement that in the limit of a homogeneous density distribution ρ_b in the bulk, the corresponding excess free-energy functional $F_{\mathrm{ex}}[\rho]$ and the direct correlation function $c^{(2)}(\mathbf{R}_1,\mathbf{R}_2)$ reduce to the known PY results. In most WDA theories one chooses an intuitive ansatz for $F[\rho]$, and tries to find suitable weights in order to fulfill the requirements mentioned above. In the LWDA, however, one exploits the simple analytic structure of c_{PY} [Eq. (2.13)], and considers the following ansatz in the bulk limit:

$$\frac{\delta^2 F_{\mathrm{ex}}[\rho]}{\rho(\mathbf{R}_1)\rho(\mathbf{R}_2)}=c_{\mathrm{PY}}(R=|\mathbf{R}_1-\mathbf{R}_2|)=\sum_{\nu=0}^{3}a_\nu(\rho)\bar{\omega}_\nu(R), \tag{2.15}$$

where the weights are chosen to be $[\omega=(\pi/6)\sigma^3]$

$$\bar{\omega}_\nu(R)=\frac{1}{8\omega}\Theta(\sigma-R)\times\begin{cases}1, & \nu=0\\ \left(1+\dfrac{3}{\nu}\right)\left(1-\dfrac{R^\nu}{\sigma^\nu}\right), & \nu=1,\ 2,\ \text{and}\ 3.\end{cases} \tag{2.16}$$

With this ansatz, Eqs. (2.15) and (2.16) determine the coefficients a_ν. In the next step it can be shown that the functional

$$F_{\mathrm{ex}}[\rho]=\sum_{\nu=0}^{3}\int d^3R\{f_\nu(\bar{\rho}_\nu(\mathbf{R}))+\tfrac{1}{2}[\rho(\mathbf{R})-\bar{\rho}_\nu(\mathbf{R})]f_\nu'(\bar{\rho}_\nu(\mathbf{R}))\}, \tag{2.17}$$

with the functions

$$\frac{\beta\omega}{\eta}f_\nu(\eta)=\begin{cases}-16+4\left(1-\dfrac{4}{\eta}\right)\ln(1-\eta), & \nu=0\\ \dfrac{3(-16+26\eta-7\eta^2)}{2(1-\eta)^2}+3\left(1-\dfrac{8}{\eta}\right)\ln(1-\eta), & \nu=1\\ 0, & \nu=2\\ \dfrac{40-68\eta+25\eta^2}{(1-\eta)^2}-8\left(1-\dfrac{5}{\eta}\right)\ln(1-\eta), & \nu=3,\end{cases} \tag{2.18}$$

fulfills both requirements stated above; i.e., reducing to $F_{PY}[\rho]$ and $c_{PY}(R)$ in the bulk limit.

The advantage of this approximation, which is called the linear weighted density approximation (LWDA) because $\bar{\rho}$ depends linearly on ρ, rests on the fact that the weights are known explicitly, and that they are independent of the *weighted* densities. Therefore, in contrast to the WDA introduced by Curtin and Ashcroft [29], one has not to solve an implicit equation for $\bar{\omega}([\bar{\rho}];|\mathbf{R}_1-\mathbf{R}_2|)$, for which the existence and uniqueness of its solution is not guaranteed. In comparison with other WDAs, which are also based on density independent weights, the LWDA differs from Tarazona's approach [30] insofar as it reproduces the PY results of a homogeneous liquid exactly, and from the method of Kierlik and Rosinberg [31] by the absence of distributions within the weights. However, one has to keep in mind that these numerical advantages are somewhat impaired by the *ad hoc* nature of the ansatz used in Eq. (2.17).

Inserting the expression for $F_{ex}[\rho]$ [Eq. (2.17)] into the definitions given in Eqs. (2.2) and (2.3), one obtains the direct correlation functions

$$c^{(1)}(\mathbf{R}_1)=-\tfrac{1}{2}\beta\sum_{\nu=0}^{3}\Big(f_\nu'(\bar{\rho}_\nu(\mathbf{R}_1))+\int d^3R\{\bar{\omega}_\nu(|\mathbf{R}_1-\mathbf{R}|)f_\nu'(\bar{\rho}_\nu(\mathbf{R}))+[\rho(\mathbf{R})-\bar{\rho}_\nu(\mathbf{R})]f_\nu''(\bar{\rho}_\nu(\mathbf{R}))\omega_\nu(|\mathbf{R}_1-\mathbf{R}|)\}\Big) \tag{2.19}$$

and

$$c^{(2)}(\mathbf{R}_1,\mathbf{R}_2)=-\sum_{\nu=0}^{3}\tfrac{1}{2}\int d^3R\{[\rho(\mathbf{R})-\bar{\rho}_\nu(\mathbf{R})]\times\beta f_\nu'''(\bar{\rho}_\nu(\mathbf{R}))\bar{\omega}_\nu(|\mathbf{R}-\mathbf{R}_1|)\bar{\omega}_\nu(|\mathbf{R}-\mathbf{R}_2|)\}+\tfrac{1}{2}\beta\{f_\nu''(\bar{\rho}_\nu(\mathbf{R}_1))+f_\nu''(\bar{\rho}_\nu(\mathbf{R}_2))\}\bar{\omega}_\nu(|\mathbf{R}_1-\mathbf{R}_2|). \tag{2.20}$$

In the following we consider hard spheres exposed to a structureless hard wall

$$V(\mathbf{R})=\begin{cases}\infty, & z<\sigma\\ 0, & z>\sigma.\end{cases} \tag{2.21}$$

This choice of the origin resembles the position $z=0$ of the nuclei of the top layer of a substrate which is composed of particles of radius $\sigma/2$. The density profile $\rho(z)$ depends only on the distance z from the wall, and all correlation functions are functions of $|\mathbf{r}_1-\mathbf{r}_2|$, z_1, and z_2, where $\mathbf{R}_i=(x_i,y_i,x_i)=(\mathbf{r}_i,z_i)$. The computational calculation requires a careful treatment of the discontinuities of these functions at $R_{12}=|\mathbf{R}_1-\mathbf{R}_2|=\sigma$. Therefore sometimes R_{12}, z_1, and z_2 are used as independent variables.

In order to obtain the total correlation function $h(\mathbf{r}_{12},z_1,z_2)$, three steps have to be carried out. First, the grand potential [Eq. (2.1)] has to be minimized in order to obtain $\rho(z)$. Then $c^{(2)}(\mathbf{r}_{12},z_1,z_2)$ can be computed via Eq. (2.20), and finally one has to invert the OZ equation (2.10).

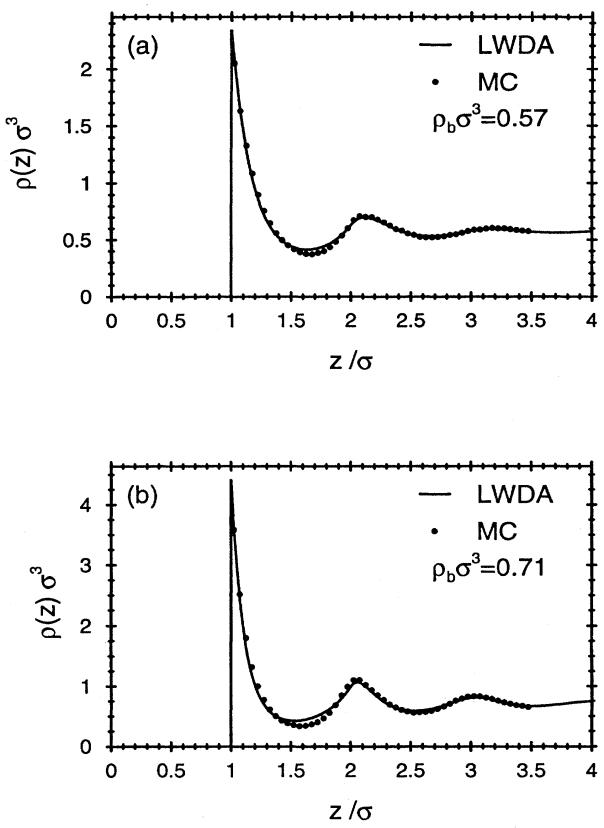

FIG. 1. Density profile of a fluid of hard spheres with diameter σ near a planar hard wall located at $z=0$ according to the LWDA density functional theory (full curve) as compared with Monte Carlo data [32] for the bulk density $\rho_b\sigma^3=0.57$ (a) and $\rho_b\sigma^3=0.71$ (b). Experimental systems are characterized by soft repulsive interaction potentials which lead to a nonzero density distribution in the depletion layer ($0<z<\sigma$) which vanishes for $z\to 0\sim\exp[-\beta V(z\to 0)]$. In the bulk freezing occurs for $\rho_b\sigma^3=0.94$ [28].

These three steps are straightforward, and computationally less demanding than the PY approach.

III. NUMERICAL RESULTS

A. Density profiles and excess coverages

The density profile $\rho(z)$ has been determined both by minimizing the grand potential functional in Eq. (2.1) and by solving the Euler-Langrage Eqs. (2.4) and (2.19). For various mesh sizes (0.02σ–0.05σ) for the integration, both approaches lead to the same profiles (see Fig. 1). These profiles satisfy the wall theorem $\rho(z=\sigma^+)=\beta p$, where p is the pressure. We find a satisfactory agreement with Monte Carlo simulations [32]. In particular the phases of the oscillations agree well. Only the first minimum appears more shallow in the analytic approach as compared with the simulation data.

The position z_n of the nth minimum of the density profile depends on the bulk density [Fig. 2(a)]. For the first minimum ($n=1$) one observes that the position z_1 [Figs. 2(a)]

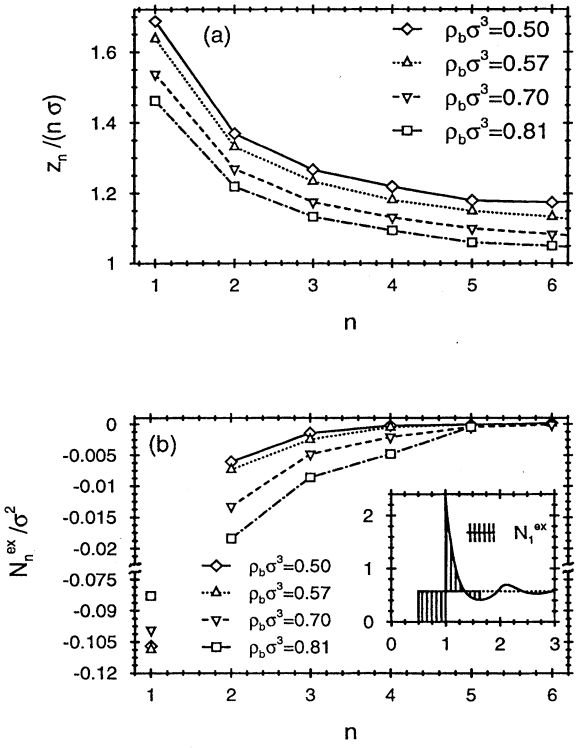

FIG. 2. For various bulk densities ρ_b of a hard sphere fluid close to a hard wall (a) shows the position of the nth minimum z_n of the density profile divided by the number n of the minimum times σ. This normalization reveals that for increasing n the distances between two successive minima tend to the hard sphere diameter σ. The inset in (b) shows $\rho(z)\sigma^3$ as function of z/σ for $\rho_b\sigma^3=0.57$ with $\rho(z\to\infty)=\rho_b$ (dotted line). Setting $z_0=\sigma/2$, these density profiles can be divided into layers where the nth layer is formed by those particles whose centers lie between z_{n-1} and z_n. Based on this definition, (b) shows the excess number density per area within each layer [Eq. (3.1)] whose geometrical meaning is indicated in the inset.

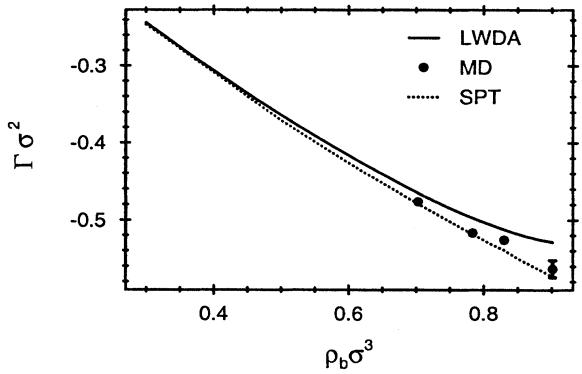

FIG. 3. Coverage Γ of a hard sphere fluid close to a hard wall. The full line corresponds to the results of the present LWDA density functional theory, and the dots denote the molecular-dynamics data [11]. [One should note that our definition of Γ (Eq. (3.2)) and that in Ref. [11] differ by $-\sigma\rho_b^3$.] The dotted line corresponds to the scaled particle theory [33]. With the exception of the highest density, the quoted error bars of the MD data are of the order of the size of the dots.

and the value $\rho(z_1)$ of the number density at this position (Fig. 1) decreases with increasing bulk density. Thus the increase of ρ_b accentuates the formation of the first layer $(z_0=\sigma/2<z<z_1)$.

A useful coarse-grained description of the density profile close to the wall consists of its division into layers where the nth layer is formed by those particles whose centers lie between the minima $n-1$ and n. For each such layer n the number density N_n per area is given by the integral of the number density profile from z_{n-1} to z_n. Since these values are close to each other, we introduce the excess number density per area

$$N_n^{\mathrm{ex}}=\int_{z_{n-1}}^{z_n} dz[\rho(z)-\rho_b]. \tag{3.1}$$

Figure 2(b) illustrates this quantity for various bulk densities. In all cases the influence of the wall decreases quickly and monotonically with increasing distance of the layer from the surface in accordance with $N_\infty^{\mathrm{ex}}=0$. The fact that N_n^{ex} is always negative confirms the expectation that the repulsive interactions between the particles and the purely repulsive substrate potential lead to a net depletion near the surface, as compared to the behavior of an ideal gas for which $\rho(z>\sigma/2)=\rho_b$.

This net depletion is also exhibited by the excess coverage

$$\Gamma(\rho)=\int_0^\infty dz[\rho(z)-\rho_b]=-\frac{\sigma}{2}\rho_b+\sum_{i=1}^{\infty} N_i^{\mathrm{ex}}, \tag{3.2}$$

which provides an important overall characterization of the density profiles. Figure 3 summarizes the results obtained from the LWDA, simulations, and the scaled particle theory (SPT) [33]. In the latter theory one assesses the work which is necessary to generate a spherical cavity in a real fluid. For a hard sphere fluid this leads to estimates of the coverage [11],

$$\Gamma_{\mathrm{SPT}}\sigma^2=\frac{9}{\pi}\frac{\eta^2}{1+2\eta}-\sigma^3\rho_b, \tag{3.3}$$

and the surface tension

$$-\beta\gamma_{\mathrm{SPT}}\sigma^2=\frac{9}{2\pi}\frac{\eta^2(1+\eta)}{(1-\eta)^3}. \tag{3.4}$$

Since the first minimum of the LWDA density profiles is somewhat too shallow, their corresponding converges are slightly higher than those predicted by simulations. The SPT underestimates Γ slightly. (The surface tension will be discussed in Sec. III D.)

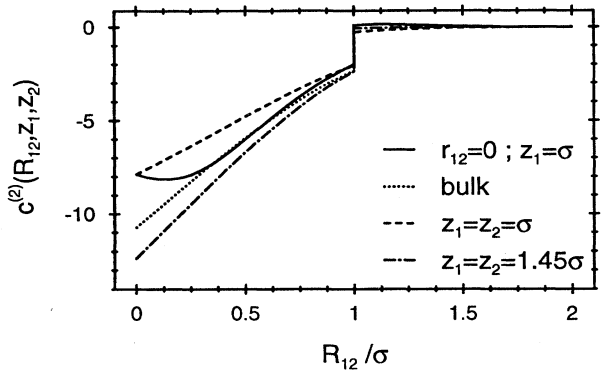

FIG. 4. The direct correlation function $c^{(2)}(r_{12},z_1,z_2)$ within the LWDA for hard spheres near a planar hard wall for the bulk density $\rho_b\sigma^3=0.57$. The dotted line corresponds to c_{PY}. The dashed and dash-dotted lines show the dependence on the lateral distance r_{12} for $z_1=z_2=\sigma$ and $z_1=z_2=1.45\sigma$, respectively, so that $R_{12}=r_{12}$. The solid curve displays the variation normal to the surface for $z_1=\sigma$ and $r_{12}=0$, so that $R_{12}=z_2-\sigma$. For the reasoning of the choices $z_1=\sigma$ and $z_2=1.45\sigma$, see Fig. 5.

B. Direct correlation functions

With the knowledge of the density profile $\rho(z)$ and the weighted densities $\bar{\rho}_\nu(z)$, the direct correlation function $c^{(2)}(\mathbf{R}_1,\mathbf{R}_2)$ follows from Eq. (2.20). Its analysis reveals that within the LWDA $c^{(2)}(\mathbf{R}_1,\mathbf{R}_2)$ vanishes for $|\mathbf{R}_1-\mathbf{R}_2|>2\sigma$, which is twice the range of the corresponding bulk function. The direct correlation function lacks a pronounced structure, and even close to the wall it is quite similar to c_{PY}. It is dimensionless, negative for $|\mathbf{R}_1-\mathbf{R}_2|<\sigma$, discontinuous at $|\mathbf{R}_1-\mathbf{R}_2|=\sigma$, and vanishes smoothly at $|\mathbf{R}_1-\mathbf{R}_2|=2\sigma$ (Fig. 4). For $R_{12}<\sigma$, Fig. 4 shows that the perturbation due to the wall is qualitatively different normal to the surface and parallel to it. Parallel to the wall the direct correlation function is a monotonically increasing function of r_{12} for all $z_1=z_2$ (see also Fig. 5), similar to the behavior of the bulk direct correlation function. However, perpendicular to the wall there is a minimum at $R_{12}\neq 0$. The discontinuity at $R_{12}=\sigma$ is determined by an analytically known functional of the equilibrium profile $\rho(z)$. Its numerical evaluation reveals that the discontinuity in $c^{(2)}(r,z_1,z_2)$ deviates from the bulk value $(-2+3\eta-\eta^3)/(1-\eta)^4$ only by 10–15 %. For $R_{12}>\sigma$ the values of $c^{(2)}(r,z_1,z_2)$ are small compared with the values for $R_{12}<\sigma$. In this region the direct correlation function of the inhomogeneous PY approximation is always zero [see Eq. (2.11)]. Figure 5 displays the deviation of $c^{(2)}(r,z_1,z_2)$ from the bulk value $c_{\mathrm{PY}}(R_{12})$. This difference vanishes quickly for increasing values $z_1=z_2$ and even at the rather high bulk density $\rho_b\sigma^3=0.81$ for $z_1,z_2<6\sigma$, $c^{(2)}(r_{12},z_1,z_2)$ can hardly be distinguished from the bulk direct correlation function. According to Eq. (2.4) the spatial dependence of the direct correlation function $c^{(1)}(\mathbf{R})$ is determined by $\ln\rho(z)$.

C. Total correlation function

With the knowledge of the direct correlation function $c^{(2)}(r_{12},z_1,z_2)$, the total correlation function $h(r_{12},z_1,z_2)$

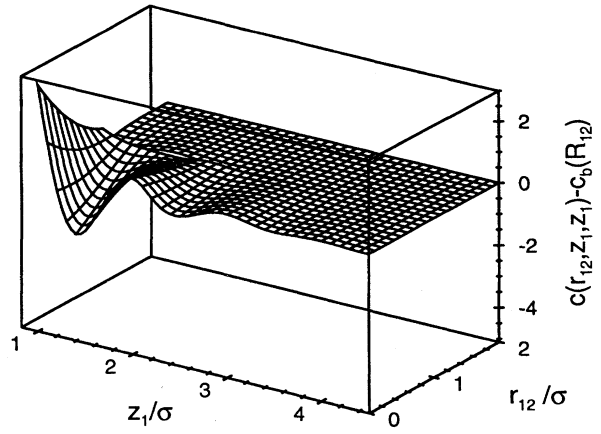

FIG. 5. The difference between the direct correlation function $c^{(2)}(r_{12},z_1,z_2)$ of a hard sphere fluid near a flat wall as obtained within the LWDA, and its bulk limit $c_{\mathrm{PY}}(R)$ as a function of r_{12} and $z_1=z_2$ at the bulk density $\rho_b\sigma^3=0.57$. The choices $z_1=0$ and $z_1=0.45\sigma$ in Fig. 4 correspond to the positions of the two extrema of $c^{(2)}(r_{12}=0,z_1=z_2)-c_{\mathrm{PY}}(R_{12}=z_1)$ closest to the wall. (The positions of these extrema do not coincide with those of the density profile.) The plotted function is discontinuous at $r_{12}=\sigma$.

follows from solving the OZ equation (2.10) by iteration. Since all correlation functions are translationally invariant in the lateral directions, the numerical computation is carried out in Fourier space with respect to the lateral coordinates,

$$h(p,z_1,z_2)=\int d^3r_1\exp^{-i\mathbf{p}(\mathbf{r}_1-\mathbf{r}_2)}h(\mathbf{R}_1,\mathbf{R}_2), \qquad (3.5)$$

and similarly for $c^{(2)}$ and $\bar{\omega}_\nu$. This leads to

$$\begin{aligned} c^{(2)}(p,z_1,z_2)=&-\tfrac{1}{2}\beta\sum_{\nu=0}^{3}\int_0^\infty dz[\rho(z)-\bar{\rho}_\nu(z)] \\ &\times f_\nu'''(\bar{\rho}_\nu(z))\bar{\omega}_\nu(p,z-z_1)\bar{\omega}_\nu(p,z-z_2) \\ &+\{f_\nu''(\bar{\rho}_\nu(z_1))+f_\nu''(\bar{\rho}_\nu(z_2))\}\bar{\omega}_\nu(p,z_1-z_2) \end{aligned} \qquad (3.6)$$

and

$$\begin{aligned} t(p,z_1,z_2)&=h(p,z_1,z_2)-c^{(2)}(p,z_1,z_2) \\ &=\int_0^\infty dz c^{(2)}(p,z_1,z)\rho(z) \\ &\quad\times[t(p,z,z_2)+c^{(2)}(p,z,z_2)]. \end{aligned} \qquad (3.7)$$

Equation (3.8) represents the OZ equation in terms of the continuous function $t(p,z_1,z_2)$. Fourier transforming it back to real space and adding $c^{(2)}(r_{12},z_1,z_2)$ as determined in Sec. III B leads to $h(r_{12},z_1,z_2)$. Using cutoffs $r_{12}^{\max}=8\sigma$ and $z^{\max}=8\sigma$, we solved the OZ equation both in real space and in lateral Fourier space, and obtained the same results.

For $z_1,z_2\gg\sigma$ the PY bulk results are reproduced. In the present model at $z_1=5\sigma$, even for a bulk density of

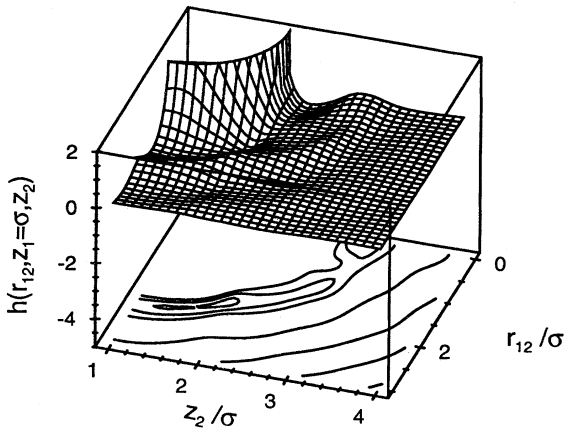

FIG. 6. Total correlation function $h(r_{12},z_1=\sigma,z_2)$ within the LWDA of a hard sphere fluid near a hard wall at the bulk density $\rho_b\sigma^3=0.81$. Values larger than 2 occurring at $R_{12}\approx\sigma$ are suppressed. (They are displayed in Fig. 7.) On the bottom of the picture we have plotted contour lines which indicate changes of h by a value of 0.1. For $R_{12}\lesssim 1.2\sigma$ these lines cannot be distinguished on the present scale, because there h varies too rapidly. Therefore the contour lines are shown only for $R_{12}\gtrsim 1.2\sigma$.

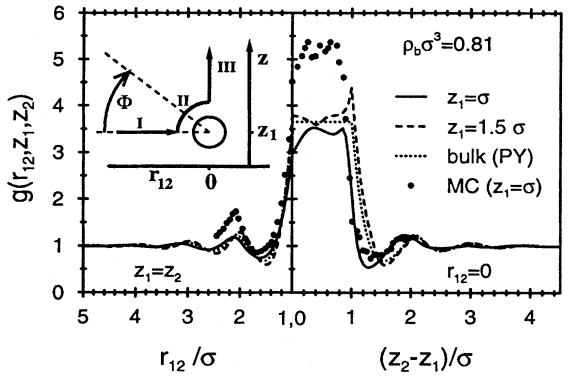

FIG. 7. The radial distribution function for hard spheres close to a planar hard wall for a bulk density $\rho_b\sigma^3=0.81$. As indicated in the inset, $g(r_{12},z_1,z_2)$ is shown in the left panel (path *I*) for $z_1=z_2$ and $r_{12}/\sigma>1$; in the middle panel (path *II*) for $R_{12}=\sigma$ and $z_1<z_2<z_1+\sigma$; and in the right panel (path *III*) for $r_{12}=0$ and $z_2>z_1+\sigma$. The full and dashed lines denote the LWDA results for $z_1=\sigma$ and $z_1=1.5\sigma$, respectively. The dotted line represents the bulk correlation function, and the dots Monte Carlo data [12] for $z_1=\sigma$. For a discussion of the comparison between the simulation data and the analytic results, see the main text. The angle Φ denotes a direction different from the paths I–III (see, cf., Fig. 13).

$\rho_b\sigma^3=0.81$ the deviations from the bulk values are less than 0.01. Hereby we used as reference an analytically exact expression of $h_{\rm PY}(R)$ available for $0<R/\sigma<5$ [24]. If one compares the PY bulk total correlation function with its counterpart obtained by simulations [15], one finds that both agree quantitatively except for R_{12} close to σ. There the PY bulk values are smaller. In view of this uncertainty of the bulk input into the LWDA, the comparison of $h(r_{12},z_1,z_2)$ with simulation data for $R_{12}\approx\sigma$ should be made in terms of the ratio of these results at the wall and the corresponding bulk reference values.

In Fig. 6, $h(r_{12},z_1,z_2)$ is shown for a bulk density of $\rho_b\sigma^3=0.81$. There, values of h larger than 2 which occur close to $|R_{12}|=\sigma$, have been omitted in order to obtain an appropriate scale for the interesting structures. One recognizes a circular structure which is interspersed by local maxima and minima. Upon reducing the bulk density this circular structure dominates the structure of the correlation function.

For a better quantitative comparison between various results it is necessary to use one-dimensional plots. To this end the following representation has proven to be useful [12]. First z_1 is taken to be equal to z_2, and $h(r_{12},z_1,z_2)$ is plotted as a function of r_{12} along the wall (path *I*). Then the distance $R_{12}=\sigma$ is fixed, and z_2 varies between σ and 2σ (path *II*). Here the total correlation function reaches it maximum. (This part was suppressed in Fig. 6.) Finally by setting $r_{12}=0$, $z_2\geq\sigma+z_1$ is moved away from the wall perpendicularly (path *II*). For small densities these plots capture most of the structure of $h(r_{12},z_1,z_2)$, so that this representation can be used for comparative purposes [12,5]; however, at higher densities additional tests are necessary.

In Ref. [12] Monte Carlo (MC) simulation data [10] are discussed using this representation. Based on these results, Fig. 7 reveals that within certain parts of paths *I–III* the Monte Carlo data lie above the LWDA results. At present one cannot tell which of them is more reliable. In the context of molecular-dynamics (MD) simulation [11], it was pointed out that the above Monte Carlo data [10] appear to be systematically too large, which is also supported by our LWDA result. The authors of Ref. [12] shared this criticism, whereby they expect that the Monte Carlo data along path *III* are more reliable than those along the other two paths. Thus we conclude that there is a fair agreement between MC data and the LWDA results as far as the phases of the oscillations are concerned, whereas the amplitudes must be tested by future simulations which are urgently needed. Along path *III* both for $\rho_b\sigma^3=0.81$ (Fig. 7) as for $\rho_b\sigma^3=0.57$ (Fig. 8), the positions of the extrema of the radial distribution func-

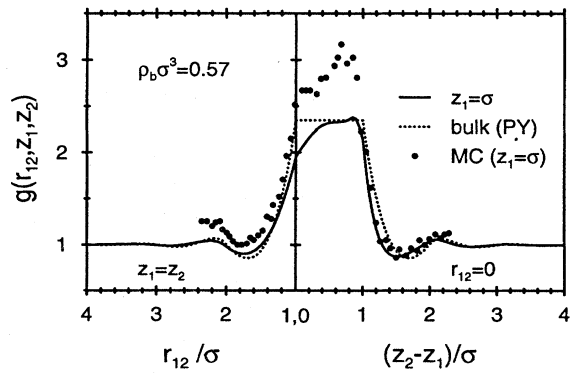

FIG. 8. The radial distribution function for hard spheres close to a planar hard wall at a bulk density of $\rho_b\sigma^3=0.57$. The representation and the meaning of the symbols are the same as in Fig. 7.

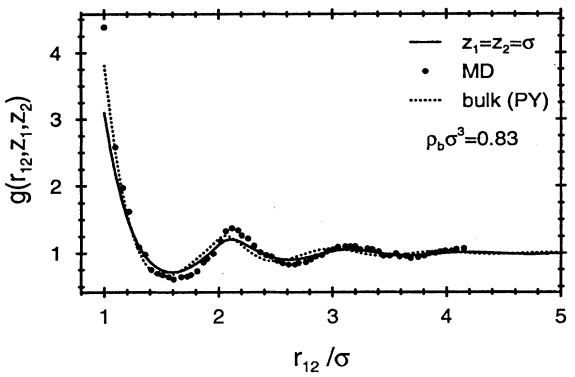

FIG. 9. The radial distribution function for hard spheres close to a planar hard wall at a bulk density of $\rho_b\sigma^3=0.83$ along path I for $z_1=z_2=\sigma$. The full line corresponds to the LWDA results, the dots denote molecular-dynamics (MD) simulation data [15]. For a comparison the dotted curve, we show $g_{\mathrm{PY}}(r_{12})$ in the bulk. In Ref. [15] these simulation data have been compared with the inhomogeneous $g_{\mathrm{PY}}(r_{12},z_1=z_2=\sigma)$, exhibiting a satisfactory agreement. In the main text the value of $g(r_{12}=\sigma,z_1=z_2)$ is denoted as $g_{ps}(z_1)$.

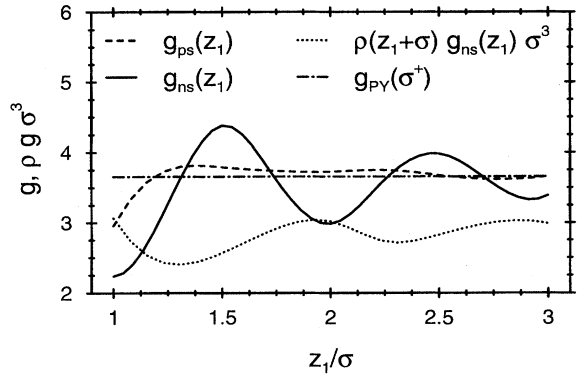

FIG. 10. Within the LWDA the contact values $g_{ps}(z_1)=g(r_{12}=\sigma,z_1=z_2)$ parallel to the surface (dashed curve) and $g_{ns}(z_1)=g(r_{12}=0,z_2=z_1+\sigma)$ normal to the surface (full curve) of the radial distribution function of a hard sphere fluid near a hard wall for a bulk density of $\rho_b\sigma^3=0.81$. The dash-dotted and dotted curves denote $g_{\mathrm{PY}}(\sigma)$ and $\rho(z_1+\sigma)g_{ns}(z_1)$, respectively. The latter curve corresponds to the contact value of the conditional singlet density [Eq. (3.8)] normal to the surface, as discussed at the end of Sec. III C (see also Fig. 13). Note that $g_{ps}(\infty)=g_{ns}(\infty)=g_{\mathrm{PY}}(\sigma)$ and $g_{ns}(\infty)\rho(\infty)=g_{\mathrm{PY}}(\sigma)\rho_b$.

tion are shifted toward smaller values of z_1 as compared with those of the bulk function $g_{\mathrm{PY}}(R)$. The comparison between Figs. 7 and 8 shows that for smaller bulk densities the agreement between MC and LWDA is better, including the amplitudes. However, as expected, close to the freezing transition ($\rho_b\sigma^3\lesssim 0.94$) the quality of the LWDA predictions for g deteriorates until even negative values for the first minimum of g appear along path *III*.

For path *I* further simulation results are available, though only for large bulk densities and for $z_1=\sigma$. In this case the oscillations of $h(r_{12},z_1,z_2)$ are more pronounced than those of $h_{\mathrm{PY}}(R_{12})$. For $\rho_b\sigma^3=0.83$, Fig. 9 compares the LWDA with simulation results [11] presented in Ref. [15]. As far as the phases of the oscillations are concerned both approaches agree rather well; however, the LWDA yields smaller amplitudes. There are simulation data available [32] even for a higher density ($\rho_b\sigma^3=0.9135$) which is close to the freezing transition $\rho_b^f\simeq 0.94$. These authors suggest interpreting the buildup of strong oscillations in $h(r_{12},z_1,z_2)$ for this density as an onset of prefreezing of the spheres near the wall. This suggestion has been confirmed and worked out by Courtemanche and van Swol [34], who found that the wall is wetted by the crystalline phase upon approaching the bulk freezing transition from the low density phase. This prefreezing seems to occur only in a close vicinity to the bulk freezing transition. As stated in the first paragraph of Sec. II B, the LWDA is unable to capture these freezing effects properly. Therefore our results are reliable only below the onset of this prefreezing phenomena. It would be very useful if in the future additional simulation data would be made available, so that the range of validity of the LWDA can be judged quantitatively in the low density regime. Furthermore it would be rewarding also to produce these simulation data for $z_1=z_2>\sigma$ because there $g(r_{12},z_1,z_2)$ exhibits a rich structure (see Fig. 7 for $z_1=1.5\sigma$).

According to Fig. 9 the difference between the LWDA and MD is largest for the contact value $g_{\mathrm{ps}}(z_1)$: $=g(r_{12}=\sigma,z_1=z_2)$. This discrepancy persists even if one compares the ratio $g_{\mathrm{ps}}^{\mathrm{LWDA}}(z_1=\sigma)/g_{\mathrm{PY}}(R=\sigma)=0.8$ with the corresponding ratio $g_{\mathrm{ps}}^{\mathrm{MD}}(z_1=\sigma)/g_{\mathrm{MD}}(R=\sigma)=0.6$ of the simulation results, where $g_{\mathrm{MD}}(R=\sigma)\equiv(\beta p_{\mathrm{MD}}/\rho_b-1)/(4\eta)$, and p_{MD} is the pressure obtained with MD. However, $g_{\mathrm{ps}}^{\mathrm{LWDA}}(z_1)$ has such a small value only close to $z_1=\sigma$. Figure 10 demonstrates that $g_{\mathrm{ps}}^{\mathrm{LWDA}}(z_1)$ increases rapidly as function of z_1, and converges to its bulk value. In contrast to that the contact value normal to the surface $g_{\mathrm{ns}}(z_1):=g(r_{12}=0,z_2=z_1+\sigma)$ attains the same bulk value very slowly and oscillatorily. This pronounced difference between the behavior at contact parallel to the surface (ps) and normal to it (ns) is remarkable. It resembles a similar behavior found in a Lennard-Jones system which was analyzed in the framework of the BGY hierarchy and the superposition approximation [35]. In this study (in which lateral contributions of the correlation function have been approximated by the bulk correlation function) the peak values of the first maximum of $g(r_{12}=0,z_1,z_2)$ as a function of z_2 for fixed z_1, which one may interpret as the correspondence of the contact values, show a similar oscillatory behavior normal to the surface.

It is rewarding to compare the LWDA with the inhomogeneous PY theory [Eq. (2.11)], because both reduce to the same homogeneous limit in the bulk. For this comparison we choose to analyze the continuous correlation function $t(\mathbf{R}_1,\mathbf{R}_2)+1=h(\mathbf{R}_1,\mathbf{R}_2)+1-c^{(2)}(\mathbf{R}_1,\mathbf{R}_2)$ [see Eq. (3.7)]. Figure 11 displays this correlation function parallel and normal to the surface within the LWDA. The values of $t+1$ along these two paths are close to each other for $R_{12}>\sigma$, where they approach their asymptotic value 1 rapidly. However, for $R_{12}<\sigma$ the values of $t+1$ differ significantly. Moreover, parallel to the surface $t+1$ exhibits a maximum at $R_{12}\approx 0.2$, whereas normal to the surface $t+1$ attains its maximum nearly linearly at $R_{12}=0$. In Fig. 2 in Ref. [13]

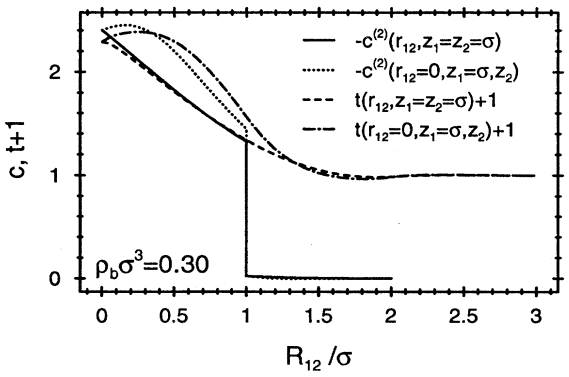

FIG. 11. Comparison between the negative direct correlation functions $-c^{(2)}(r_{12},z_1,z_2)$ for $z_1=z_2=\sigma$ and for $r_{12}=0$ and $z_1=\sigma$, respectively, with $t(r_{12},z_1,z_2)+1=h(r_{12},z_1,z_2)+1-c^{(2)}(r_{12},z_1,z_2)$ [Eq. (3.7)] as obtained within the LWDA. In an exact theory the full curve and dashed curves as well as the dotted and dash-dotted curves coincide for $R_{12}=\sqrt{r_{12}^2+(z_1-z_2)^2}<\sigma$. The LWDA violates this slightly. This violation is largest for the present case $z_1=\sigma$, and disappears rapidly for increasing values of z_1.

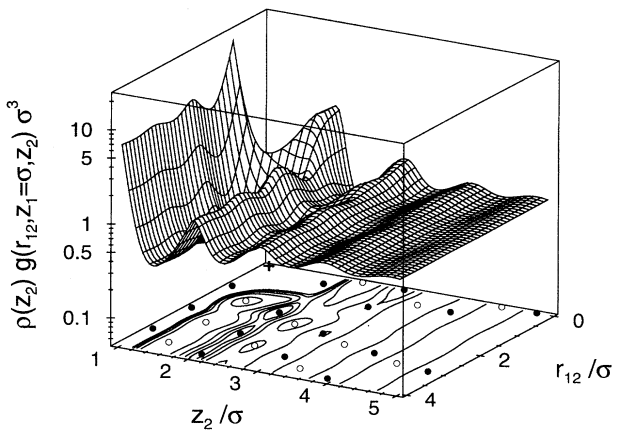

FIG. 12. The conditional singlet density $\rho(\mathbf{R}_2|\mathbf{R}_1)=\rho(z_2)g(r_{12},z_1=\sigma,z_2)$ within the LWDA of a hard sphere fluid near a hard wall at a bulk density $\rho_b\sigma^3=0.81$. It corresponds to the density distribution of a hard sphere fluid exposed to a hard half sphere sitting on top of a hard planar wall. The circles and the dots in the contour line plot at the bottom denote the positions of the local minima and maxima, respectively. Note the logarithmic scale of the ordinate. Close to the wall and to the half sphere, $\rho(\mathbf{R}_2|\mathbf{R}_1)$ varies so rapidly that we have omitted the contour lines for $\rho(\mathbf{R}_2|\mathbf{R}_1)\sigma^3>1.3$. From one contour line to the next $\rho(\mathbf{R}_2|\mathbf{R}_1)$ varies by an amount of $0.2\sigma^{-3}$. The cross denotes the position $\mathbf{R}_1$ of the center of the fixed half-sphere.

this correlation function $t+1$ as obtained by the PY theory (within which $t+1$ equals the cavity function y by construction, which is neither the case within the LWDA nor in general) is shown for the same density and representation as in Fig. 11. By inspection one observes an almost quantitative agreement, which we find to persist even at higher densities, as one can infer from Ref. [15].

In addition, Fig. 11 allows us to investigate to what extent LWDA violates the exact relation $h(\mathbf{R}_1,\mathbf{R}_2)=-1$ for $R_{12}<\sigma$, i.e., $t+1=-c^{(2)}$. By comparing the full curve with the dashed one and the dotted curve with the dash-dotted one, respectively, one finds that parallel to the surface there is only a slight violation, whereas normal to the surface this is more pronounced. To our knowledge there is no *a priori* reason that any WDA fulfills this requirement from the outset. (Below we shall point out a possibility to overcome this difficulty.) We find that this violation, i.e., $h+1\neq 0$ for $R_{12}<\sigma$, disappears rapidly for $z_1\gg\sigma$.

The physical understanding of the total correlation function is facilitated by resorting to Percus' test particle theorem [36]. If Σ denotes a semi-infinite fluid exposed to a substrate, and Σ' the same kind of fluid exposed to the same substrate but in addition with a fluid particle fixed at a position $\mathbf{R}_1$ in front of this substrate, the test particle theorem states that the one-point correlation function of the number density in Σ', the so-called conditional singlet density [37] $\rho_{\Sigma'}(\mathbf{R}_2|\mathbf{R}_1)$, which depends on $\mathbf{R}_2$ and parametrically on $\mathbf{R}_1$, can be expressed in terms of the number density and the total correlation function h of the system Σ:

$$\rho_{\Sigma'}(\mathbf{R}_2|\mathbf{R}_1)=\rho_\Sigma(\mathbf{R}_2)[h_\Sigma(\mathbf{R}_1,\mathbf{R}_2)+1]. \tag{3.8}$$

Thus in the present case the product $\rho(z_2)[h(r_{12},z_1,z_2)+1]=\rho(z_2)g(r_{12},z_1,z_2)$ describes the number density distribution of a hard sphere fluid which is exposed to an environment consisting of a hard planar wall and a hard sphere of radius σ fixed at the point $\mathbf{R}_1$ in front of the wall. Based on our knowledge of h_Σ and ρ_Σ, Fig. 12 shows how the presence of the sphere fixed at $r_{12}=0$ and $z_2=\sigma$ perturbs the translationally invariant density profile in the system Σ. The location of the local extrema of $\rho(\mathbf{R}_2|\mathbf{R}_1)$ are distributed rather regularly. Approximately this can be understood as the superposition of the oscillatory density distribution around a fixed particle in the bulk, and the oscillatory density variation near a planar wall. This checks with the fact that the extrema of the density profile $\rho_\Sigma(z_2)$ and the values of z_2 of the extrema of $\rho(\mathbf{R}_2|\mathbf{R}_1)$ almost coincide (see Table I). In accordance with the fact that for decreasing number densities the position of the first minimum of $\rho_\Sigma(z_2)$ shifts to larger values of z_2, one finds the same for $\rho(\mathbf{R}_1|\mathbf{R}_2)$. Thus the influence of the perturbation induced by the fixed sphere is mainly reflected in the lateral positions r_{12} of these extremas. The content of Figs. 7 and 8 and of Table I characterizes the structure of the total correlation function well, and offers a good opportunity for a comparison with future simulation studies.

The conditional singlet density $\rho(\mathbf{R}_2|\mathbf{R}_1)$ also allows one to shed additional light onto the mechanism leading to the oscillatory density profile near the wall (Fig. 1). To this end we consider the first BGY equation [Eq. (2.12)], which expresses the force balance at a point $\mathbf{R}_1$ between the external force $-\nabla V(\mathbf{R}_1)$, the force resulting from the interaction potentials of the fluid particles around $\mathbf{R}_1$ which contains $\rho(\mathbf{R}_2|\mathbf{R}_1)$, and the entropic repulsion given by $\rho^{-1}(\mathbf{R}_1)\nabla_{\mathbf{R}_1}\rho(\mathbf{R}_1)$. In the absence of an external potential $[V(\mathbf{R})=0]$ the fluid is homogeneous ($\rho=$const), so that in spite of $\rho(\mathbf{R}_2|\mathbf{R}_1)>0$ the integral in Eq. (2.12) vanishes due to the symmetry and the vector character of the integrand.

TABLE I. Positions of and values at the extrema of the conditional singlet density $\rho(\mathbf{R}_2|\mathbf{R}_1)$ [Eq. (3.8)] for $z_1=\sigma$, $z_2<2.7\sigma$, and $r_{12}<3.7\sigma$ within the LWDA (see Fig. 12). z_ρ denotes the location of the extrema of the density profile. Note that the values for z_ρ and z_2 are rather close.

$\rho_b\sigma^3=0.81$							
minima				maxima			
z_ρ/σ	z_2/σ	r_{12}/σ	$\rho(\mathbf{R}_2\|\mathbf{R}_1)\sigma^3$	z_ρ/σ	z_2/σ	r_{12}/σ	$\rho(\mathbf{R}_2\|\mathbf{R}_1)\sigma^3$
0.45	0.45	1.48	0.27	0.00	0.00	1.00	20.06
	0.45	2.56	0.36		0.00	2.10	8.02
	0.45	3.57	0.39		0.00	3.15	7.08
1.45	1.35	0.00	0.34	1.05	0.95	0.31	3.36
	1.45	2.04	0.52		1.05	1.70	1.70
	1.45	3.13	0.55		1.05	2.76	1.51
2.40	2.40	0.49	0.65	2.00	1.95	0.00	1.23
					1.90	0.89	1.06
	2.40	2.48	0.68		1.95	2.21	1.07
	2.40	3.69	0.68		2.00	3.35	1.04

$\rho_b\sigma^3=0.57$							
minima				maxima			
z_ρ/σ	z_2/σ	r_{12}/σ	$\rho(\mathbf{R}_2\|\mathbf{R}_1)\sigma^3$	z_ρ/σ	z_2/σ	$r12/\sigma$	$\rho(\mathbf{R}_2\|\mathbf{R}_1)\sigma^3$
0.65	0.65	1.62	0.35	0.00	0.00	1.00	4.57
	0.65	2.72	0.41		0.00	2.25	2.44
	0.65	3.79	0.41		0.00	3.35	2.36
1.65	1.60	0.00	0.47	1.10	1.00	0.00	1.34
	1.65	2.14	0.52		1.10	1.85	0.74
	1.65	3.37	0.53		1.10	3.06	0.70
2.70	2.65	0.00	0.55	2.10	2.15	0.00	0.63
	2.70	2.53	0.56		2.15	2.37	0.60
					2.15	3.67	0.60

This corresponds to the fact that in a homogeneous fluid the forces due to the fluid particles surrounding a point $\mathbf{R}_1$ are radially symmetric, and thus compensate each other in opposing directions. If, however, the translational symmetry is destroyed, e.g., by the presence of a wall, there are less particles to the left of $\mathbf{R}_1$ than to the right, which leads to an imbalance of these forces, i.e., the integral in Eq. (2.12) does not vanish. Therefore the total force balance is accomplished by a spatially varying density profile.

This general mechanism which is of current interest [37] can be followed in detail for the present model system of hard spheres. By studying the smooth cavity function $y(\mathbf{R})$ the limiting case of a hard sphere interaction potential leads from Eq. (2.12) to [16]

$$-\frac{1}{\rho(z_1)}\frac{\partial}{\partial z_1}\rho(z_1)=-\beta\frac{\partial}{\partial z_1}V(z_1)-2\pi\int_{z_1-\sigma}^{z_1+\sigma}dz_2\rho(z_2)\times g(R_{12}=\sigma,z_1,z_2)(z_1-z_2). \quad (3.9)$$

In this case the influence of the aforementioned imbalance of the internal forces on the density profile can be analyzed in terms of the pressure. At a *hard* wall the pressure is given by the product of the probability that a particle hits the wall, which is proportional to $\rho(z=\sigma^+)$ and a factor determined by the momentum distribution. Since in classical statistical mechanics the momentum distribution is independent of the interaction potential between the particles, it follows from that of an ideal gas. Based on the equation of state $\beta p=\rho_b$, one is led to the wall theorem $\beta p=\rho(z=\sigma^+)$, which can be proven more generally and rigorously [36]. The relative value of $\rho(z=\sigma^+)$ compared with ρ_b depends on the interaction potential between the fluid particles. If it is predominantly attractive the density at the hard wall will be smaller than ρ_b, and drying will occur [8]. In the present case of a hard sphere fluid Fig. 13 shows that at the wall the imbalance of the internal forces leads to a net force directed toward the wall, resulting in $\rho(z=\sigma^+)>\rho_b$. In accordance with Eq. (3.9) this corresponds to a negative gradient of $\rho(z)$ at $z=\sigma^+$ (compare Fig. 1). Thus these force considerations demonstrate why the density distribution of a hard sphere fluid exhibits a sharp maximum at a hard wall. The dotted curve in Fig. 10 shows how the value of the dashed curve in Fig. 13 at $\Phi=90°$ varies if one moves with z_1 away from the surface $z_1=\sigma$. Thus the oscillations of this value as a function of z_1 signals that one also has to face oscillations in the density profile, which is in accordance with Fig. 1. Therefore the force distribution in this inhomogeneous fluids allows a helpful insight into the mechanism behind the density distribution close to the wall. Furthermore these considerations are useful in the context of driving additional approximation schemes for the description of inhomogeneous fluids [37].

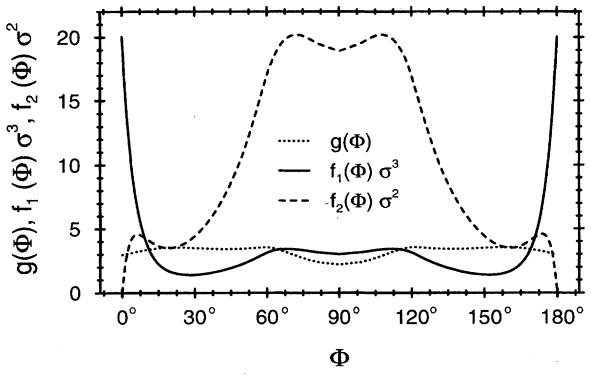

FIG. 13. Three correlation functions related to the radial distribution function of a hard sphere fluid close to a planar hard wall for the bulk density $\rho_b\sigma^3=0.81$. Based on the notation in the inset of Fig. 7, the correlations are shown for $|R_{12}|=\sigma$ as function of the angle Φ which denotes the deviation from the direction parallel to the wall ($z_2=z_1+\sigma\sin\Phi$). The dotted line corresponds to $g(\Phi):=g(R_{12}=\sigma,z_1=\sigma,z_2=z_1+\sigma\sin\Phi)$ which is also shown in the middle panel of Fig. 7. The full line denotes the conditional singlet density $f_1(\Phi):=\rho(z_2=z_1+\sigma\sin\Phi)g(R_{12}=\sigma,z_1=\sigma,z_2=z_1+\sigma\sin\Phi)$ which is also shown in Fig. 12 where it corresponds to that part of the boundary of the two-dimensional plotted surface which is adjacent to the back left edge of the cube. The dashed curve denotes the integrand $f_2(\Phi):=2\pi f_1(\Phi)\sigma\sin\Phi$ of the integral appearing in Eq. (3.9). Thus the area under the curve $f_2(\Phi)$ measures up to the minus sign, the net force acting on the test particle at $z_1=\sigma$. The variation of $f_2(90°)$ as a function of z_1 is displayed as the dotted curve in Fig. 10.

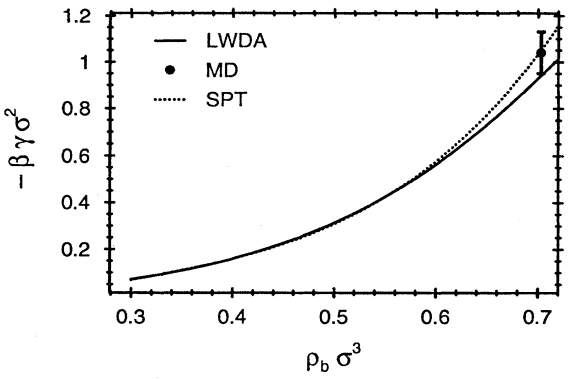

FIG. 14. Surface tension of a hard sphere fluid close to a hard wall. The full line denotes the results of the LWDA, and the dot those of molecular-dynamics simulations [11], and the dotted line corresponds to the scaled particle theory [33].

D. Surface tensions

From the previous subsections it is apparent that a thorough discussion of the two-point correlation function is aggravated by the fact that it depends on four variables: r_{12}, z_1, z_2, and ρ_b. Therefore it is very useful to consider not only the local but also the global properties of a liquid close to a wall. There are two global quantities which are of experimental interest: the excess coverage, which has been discussed in Sec. III A, and is accessible by gravimetric measurements; and the surface tension γ which, for example, is important for contact angles [8]. Via the exact sum rule [19]

$$\beta\gamma=\tfrac{1}{4}\int_0^\infty dz_1\int_0^\infty dz_2\int_{\mathbb{R}^2}d^2r_{12}\rho'(z_1)\rho'(z_2)r_{12}^2 \times c^{(2)}(r_{12},z_1,z_2), \tag{3.10}$$

it can be expressed in terms of the direct correlation function and the derivate of the density profile $\rho(z)=\rho_+(z)\Theta(z-\sigma)$, where $\rho_+(\sigma)=\rho(\sigma^+)$. Figure 14 shows that for $\rho_b\sigma^3\lesssim 0.6$ the predictions of the LWDA are very close to those of the SPT [Eq. (3.3)]. For larger values of ρ_b the LWDA yields smaller values, also in comparison with simulation data. For even larger values of ρ_b the numerical accuracy of evaluating Eq. (3.10) deteriorates because therein the derivative of $\rho(z)=\rho_+(z)\Theta(z-\sigma)$ generates differences of large numbers. In this regime it seems to be appropriate to obtain the surface tension as the surface contribution to Eq. (2.1) by subtracting the bulk term and performing the thermodynamic limit. We defer the analysis of this alternative approach to a future study, which is also planned to include attractive interactions. According to Fig. 4 the direct correlation function near the wall does not differ dramatically from its bulk form. Thus one may be inclined to surmise that in Eq. (3.10) the derivative of the density profile contains the most relevant interfacial property in determining γ. However, by checking this idea one finds that this replacement leads to values of γ which are twice as high as the proper ones. Therefore the relatively small differences between $c^{(2)}(r_{12},z_1,z_2)$ and its bulk value turn out to have a strong influence on global quantities like the surface tension. Thus a detailed quantitative understanding of the interfacial two-point correlation function is indispensable.

IV. SUMMARY

We have obtained the following main results for the structure of hard spheres close to a hard wall.

(1) Within a recently introduced linear weighted density approximation (LWDA) the number density profile close to the wall has been determined. There is a satisfactory agreement with published Monte Carlo data (Fig. 1).

(2) A coarse-grained description of the density profiles reveals the depletion of the particles close to the wall (Fig. 2).

(3) Apart from the bulk densities close to the freezing transition, the predictions of the LWDA for the excess coverage (Fig. 3) and the surface tension (Fig. 14) are close to those of the scaled particle theory and simulations.

(4) Within the LWDA we have determined the inhomogeneous direct correlation function, which differs from its bulk form only rather close to the surface (Figs. 4 and 5).

(5) Based on these results we have solved the Ornstein-Zernicke equation for the total correlation function $h(\mathbf{R}_1,\mathbf{R}_2)$. Upon increasing the bulk density, its dominant circular structure is enriched by the pronounced formation of local maxima and minima (Fig. 6). A detailed comparison with published simulation data reveals a satisfactory agreement with respect to the phases of the oscillatory structure of the radial distribution function $g(\mathbf{R}_1,\mathbf{R}_2)=h(\mathbf{R}_1,\mathbf{R}_2)+1$, but discrepancies for certain amplitudes (Figs. 7–9). There are indications that an understanding of these differences require improved simulation data.

(6) Based on the test particle theorem the radial distribution function allows one to analyze in detail the conditional singlet density $\rho(\mathbf{R}_2|\mathbf{R}_1)=\rho(\mathbf{R}_2)g(\mathbf{R}_1,\mathbf{R}_2)$. The extrema of this correlation function (Fig. 12 and Table I) are well suited to compare future studies involving different approaches for this model system.

(7) Within the framework of the Born-Green-Yvon equation (2.12) the knowledge of the conditional singlet density enables one to analyze in detail the balance of forces acting on a test particle close to the wall [see Eq. (3.9) and the discussion thereafter]. This enhances the understanding of the layering in the density profile close to the wall.

Within the LWDA the total correlation function violates the exact relation $h(R_{12}<\sigma,z_1,z_2)=-1$. Most probably this deficiency is shared by all other presently available weighted density functional theories. We want to point out that the test particle theorem [Eq. (3.8)] offers the possibility to overcome this problem. If one directly computes the one-point correlation function of the number density for a fluid exposed to a substrate plus a fixed particle by minimizing the grand potential functional for such a configuration, and divides this by the corresponding density profile in the absence of the fixed particle, one obtains $h(\mathbf{R}_1,\mathbf{R}_2)+1$, which fulfills the above requirement by construction. However, this minimization procedure requires a substantial numerical effort.

[1] L. Mailänder, H. Dosch, J. Peisl, and R. L. Johnson, Phys. Rev. Lett. **64**, 2527 (1990); H. Dosch, L. Mailänder, R. L. Johnson, and J. Peisl, Surf. Sci. **279**, 367 (1992); H. Dosch, *Critical Phenomena at Surfaces and Interfaces: Evanescent X-Ray and Neutron Scattering*, Springer Tracts in Modern Physics, Vol. 126 (Springer, Heidelberg, 1992).

[2] S. Dietrich and H. Wagner, Phys. Rev. Lett. **51**, 1469 (1983); Z. Phys. B **56**, 207 (1984).

[3] For further experimental steps in this direction for fluid systems see, e.g., M. K. Sanyal, S. K. Sinha, K. G. Huang, and B. M. Ocko, Phys. Rev. Lett. **66**, 628 (1991); O. H. Seeck, P. Müller-Buschbaum, M. Tolan, and W. Press, Europhys. Lett. **29**, 699 (1995).

[4] S. Dietrich and A. Haase, Phys. Rep. **260**, 1 (1995).

[5] S. Sokolowski and J. Fischer, J. Chem. Phys. **96**, 5441 (1991).

[6] P. Tarazona, Surf. Sci. **331-333**, 989 (1995).

[7] R. Evans, in *Fundamentals of Inhomogeneous Fluids*, edited by D. Henderson (Dekker, New York, 1992), p. 85.

[8] S. Dietrich, in *Phase Transitions and Critical Phenomena*, edited by C. Domb and J. Lebowitz (Academic, London, 1988), Vol. 12, p. 1; M. Schick, in *Liquids at Interfaces*, Les Houches Summer School Lectures, Session XLVIII, edited by J. Chavrolin, J. F. Joanny, and J. Zinn-Justin (Elsevier, Amsterdam, 1990), p. 415.

[9] G. Nägele, Habilitation thesis, University of Constance, 1994 (unpublished); R. Klein and B. D. Aguanno (unpublished).

[10] I. K. Snook and D. Henderson, J. Chem. Phys. **68**, 2134 (1978).

[11] J. R. Henderson and F. van Swol, Mol. Phys. **51**, 991 (1984).

[12] D. Henderson and M. Plischke, Proc. R. Soc. London Ser. A **400**, 163 (1985).

[13] S. Sokolowski, J. Chem. Phys. **73**, 3507 (1980).

[14] M. Plischke and D. Henderson, J. Phys. Chem. **88**, 6544 (1984).

[15] M. Plischke and D. Henderson, Proc. R. Soc. London Ser. A **404**, 323 (1986).

[16] R. Kjellander and S. Sarman, J. Chem. Soc. Faraday Trans. **87**, 1869 (1991).

[17] G. P. Brenan and R. Evans, Mol. Phys. **73**, 789 (1991).

[18] A. R. Denton and N. W. Ashcroft, Phys. Rev. A **44**, 1219 (1991).

[19] R. Evans, Adv. Phys. **28**, 143 (1979).

[20] J. P. Hansen and I. R. Mc Donald, *Theory of Simple Liquids* (Academic, London, 1986).

[21] D. Henderson, in *Fundamentals of Inhomogeneous Fluids*, edited by D. Henderson (Dekker, New York, 1992), p. 177.

[22] S. Sokolowski, Mol. Phys. **49**, 1481 (1983).

[23] M. Wertheim, Phys. Rev. Lett. **10**, 321 (1963).

[24] W. R. Smith and D. Henderson, Mol. Phys. **19**, 411 (1970).

[25] P. Tarazona and R. Evans, Mol. Phys. **47**, 1033 (1982).

[26] A. O. Parry and R. Evans, Mol. Phys. **65**, 455 (1988).

[27] R. Ohnesorge, Ph.D. thesis, University of Munich, 1994.

[28] W. G. Hoover and F. H. Ree, J. Chem. Phys. **49**, 3608 (1968).

[29] W. A. Curtin and N. W. Ashcroft, Phys. Rev. A **32**, 2909 (1985); Phys. Rev. Lett. **56**, 2775 (1986).

[30] P. Tarazona, Phys. Rev. A **31**, 2672 (1985); **32**, 3148 (1985).

[31] E. Kierlik and M. Rosinberg, Phys. Rev. A **42**, 3382 (1990).

[32] R. D. Groot, N. M. Faber, and J. P. v. d. Eerden, J. Chem. Phys. **62**, 861 (1987).

[33] H. Reiss, H. L. Frisch, E. Helfand, and J. L. Lebowitz, J. Chem. Phys. **32**, 119 (1960).

[34] D. J. Courtemanche and F. van Swol, Phys. Rev. Lett. **69**, 2078 (1992).

[35] B. Borštnik and D. Janežič, Mol. Phys. **50**, 1199 (1983).

[36] J. R. Henderson, in *Fundamentals of Inhomogeneous Fluids* (Ref. [21]), p. 23.

[37] J. D. Weeks, R. L. B. Selinger, and J. Q. Broughton, Phys. Rev. Lett. **75**, 2694 (1995).